THE JOURNAL OF PHYSICAL CHEMISTRY Letters

Letter

Cite This: J. Phys. Chem. Lett. 2019, 10, 7062−7070

pubs.acs.org/JPCL

Quasi-Diabatic Scheme for Nonadiabatic On-the-Fly Simulations

Wanghuai Zhou,[†,‡] Arkajit Mandal,[‡] and Pengfei Huo*[,‡]

[†]Advanced Functional Material and Photoelectric Technology Research Institution, School of Science, Hubei University of Automotive Technology, Shiyan, Hubei 442002, People's Republic of China

[‡]Department of Chemistry, University of Rochester, 120 Trustee Road, Rochester, New York 14627, United States

Supporting Information

We use the quasi-diabatic (QD) propagation scheme to perform on-the-fly nonadiabatic simulations of the photodynamics of ethylene. The QD scheme enables a seamless interface between accurate diabatic-based quantum dynamics approaches and adiabatic electronic structure calculations, explicitly avoiding any efforts to construct global diabatic states or reformulate the diabatic dynamics approach to the adiabatic representation. Using the partial linearized path-integral approach and the symmetrical quasi-classical approach as the diabatic dynamics methods, the QD propagation scheme enables direct nonadiabatic simulation with complete active space self-consistent field on-the-fly electronic structure calculations. The population dynamics obtained from both approaches are in a close agreement with the quantum wavepacket-based method and outperform the widely used trajectory surface-hopping approach. Further analysis of the ethylene photodeactivation pathways demonstrates the correct predictions of competing processes of nonradiative relaxation mechanism through various conical intersections. This work provides the foundation of using accurate diabatic dynamics approaches and on-the-fly adiabatic electronic structure information to perform ab initio nonadiabatic simulation.

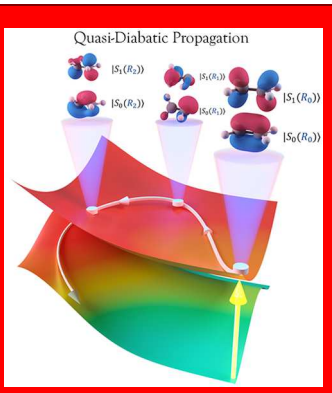

Nonadiabatic molecular dynamics (NAMD) simulation plays an indispensable role in investigating photochemical and photophysical processes of molecular systems.[1−7] The essential task of NAMD[1] is to solve the coupled electronic−nuclear dynamics governed by the total Hamiltonian of the molecular system

$$\hat{H} = \hat{T} + \hat{V}(r, R) \tag{1}$$

where r and R represent the electronic and nuclear degrees of freedom (DOF), respectively; $\hat{T} = -\frac{\hbar^2}{2M}\nabla_R^2$ is the nuclear kinetic energy operator, and $\hat{V}(r,R)$ is the electronic Hamiltonian operator that describes the kinetic energy of electrons and electron−electron, nuclear−nuclear, as well as electronic−nuclear interactions.

Rather than directly solving the time-dependent Schrödinger equation (TDSE) governed by $\hat{H}$, NAMD simulation is often accomplished[1,2] by performing on-the-fly electronic structure calculations that provide the energy and gradients and the quantum dynamics simulations that propagate the motion of the nuclear DOFs (described by trajectories or nuclear wave functions). In particular, the electronic structure calculations solve the eigenequation

$$\hat{V}(r, R)|\Phi_\alpha(R)\rangle = E_\alpha(R)|\Phi_\alpha(R)\rangle \tag{2}$$

which provides the *adiabatic* state $|\Phi_\alpha(R)\rangle$ and energy $E_\alpha(R)$.

Because of the readily available electronic structure information in the *adiabatic* representation, quantum dynamics approaches formulated in this representation have been extensively used to perform on-the-fly NAMD simulations, including the popular fewest-switches surface hopping (FSSH),[4,8−15] ab initio multiple spawning (AIMS),[3,7,16] and several recently developed Gaussian wavepacket approaches,[17−21] coupled-trajectory approaches,[22−25] and the ab initio multiconfiguration time-dependent Hartree (MCTDH) approach.[26−30] Among them, FSSH is one of the most popular approaches in NAMD, which uses mixed quantum-classical (MQC) treatment of the electronic and nuclear DOFs that provide efficient nonadiabatic simulation. As a MQC method, however, FSSH treats quantum and classical DOFs on different footings,[1] generating artificial electronic coherence[8,12] that could give rise to incorrect chemical kinetics[12] or the breakdown of the detailed balance.[31] Recently developed nonadiabatic quantum dynamics approaches[32−42] have shown great promise to address the deficiency and limitations of the MQC approximation. However, these approaches are usually developed in the *diabatic* representation and are incompatible with the available adiabatic electronic structure calculations. Reformulating them back to the adiabatic representation requires additional and sometimes nontrivial theoretical efforts. One common strategy to address this challenge is constructing global diabatic states.[2,43−48] Another related direction is to build the "on-the-fly" diabatic state through a diabatization procedure,[28−30] which has enabled ab initio quantum dynamics calculations for

Received: September 17, 2019
Accepted: October 31, 2019
Published: October 31, 2019

DOI: 10.1021/acs.jpclett.9b02747
J. Phys. Chem. Lett. 2019, 10, 7062−7070

the variational multiconfiguration Gaussian method[49] and the direct-dynamics MCTDH approach.[26−30]

We have developed the quasi-diabatic (QD) propagation scheme[50,51] to address this challenge from an alternative perspective, which avoids performing *any* explicit diabatization procedure. The central idea behind the QD scheme is realizing that to propagate quantum dynamics with diabatic dynamics approaches one needs only *locally* well-defined diabatic states, and these local diabatic states can simply be adiabatic states with a reference geometry (which are commonly referred to as the crude adiabatic states). We emphasize that this idea is fundamentally different from the quasi-diabatization procedure[52,53] or the propagation-based diabatization,[30,49] which requires the explicit adiabatic to diabatic transformation. The QD scheme[50] directly uses the adiabatic states associated with a reference geometry as the local diabatic states during a short-time quantum propagation and dynamically updates the definition of the QD states along the time-dependent nuclear trajectory. Historically, this scheme was introduced to propagate the electronic amplitudes in surface-hopping simulations[9,54−57] (which is commonly referred to as the "local diabatic" basis approach). It has also been used in Gaussian wave packet dynamics approaches,[18−21,58] which is termed the "moving crude adiabatic" scheme.[20] In the context of our QD propagation scheme, we use the "moving crude adiabatic states" as the local diabatic state to address the discrepancy between the diabatic quantum dynamics approaches and adiabatic electronic structure calculations.[50] It allows a direct interface between diabatic dynamics approaches with adiabatic electronic structure calculations. It also enables using realistic ab initio test cases to assess the accuracy and limitations of recently developed quantum dynamics approaches.[59]

In this Letter, we provide an ab initio on-the-fly example of using the QD scheme[50] for nonadiabatic simulations with a *diabatic* quantum dynamics approach and the adiabatic electronic structure calculations. In particular, we use two recently developed diabatic dynamics approaches[33,60] to perform on-the-fly NAMD simulations of the well-studied ethylene photodynamics. On-the-fly electronic structure calculations are performed at the level of the complete active space self-consistent field (CASSCF) approach. The results obtained from these quasi-diabatic quantum dynamics simulations are in close agreement with the AIMS approach.[3] Thus, this Letter provides the first on-the-fly example of the QD propagation scheme and completes the establishment of it in the field of ab initio nonadiabatic dynamics as a powerful tool to enable accurate diabatic quantum dynamics approaches for on-the-fly simulations.

Theoretical Approach. In this work, we demonstrate that the QD scheme enables a direct interface between *diabatic* dynamics approaches and *adiabatic* electronic structure calculations. In particular, we use the partial-linearized density matrix (PLDM) path-integral approach,[5,33] as well as the symmetrical quasi-classical (SQC) approach[60] as the diabatic dynamics approach. Both methods are originally developed in the diabatic representation and are based on the Meyer−Miller−Stock−Thoss[61−63] (MMST) mapping representation. Here, we briefly summarize the PLDM approach, whereas the SQC approach is discussed in the Supporting Information.

PLDM is an approximate quantum dynamics method based on the real-time path-integral approach.[33] Using the MMST mapping representation,[63] the nonadiabatic transitions among discrete electronic states $\{|i\rangle, |j\rangle\}$ are exactly mapped[63] onto the phase-space motion of the fictitious variables through the relation $|i\rangle\langle j| \rightarrow \hat{a}_i^\dagger \hat{a}_j$, where $\hat{a}_i^\dagger = (\hat{q}_i - i\hat{p}_i)/\sqrt{2}$ and $\hat{a}_i = (\hat{q}_i + i\hat{p}_i)/\sqrt{2}$. After performing the linearization approximation on the nuclear DOFs, we obtain the following PLDM reduced density matrix:[33]

$$\begin{aligned}\rho_{ij}(t) &= \mathrm{Tr}_R[\hat{\rho}(0)e^{i\hat{H}t/\hbar}|i\rangle\langle j|e^{-i\hat{H}t/\hbar}] \\ &\approx \sum_{kl}\int d\tau[\hat{\rho}(0)_{kl}^{W}]T_{ki}(t)T'_{jl}(t)\end{aligned} \tag{3}$$

where $\int d\tau \equiv \frac{1}{2\pi\hbar}\int dRdPd\mathbf{q}d\mathbf{p}d\mathbf{q}'d\mathbf{p}'G_0G'_0$ represents the phase space integration for all DOFs; G_0 and G'_0 represent coherent state distribution of mapping oscillators; $T_{ki}(t) = \frac{1}{2}(q_i(t) + ip_i(t))(q_k(0) - ip_k(0))$ and $T'_{jl}(t) = \frac{1}{2}(q'_l(0) + ip'_l(0))(q'_j(t) - ip'_j(t))$ are the electronic transition amplitudes associated with the forward mapping trajectory $\{\mathbf{q}, \mathbf{p}\}$ and the backward mapping trajectory $\{\mathbf{q}', \mathbf{p}'\}$, respectively. $[\hat{\rho}(0)_{kl}^{W}]$ is the partial Wigner transform (with respect to the nuclear DOFs) of the kl^{th} matrix element of the initial total density operators $\hat{\rho}(0)$.

Classical trajectories are used to evaluate the approximate time-dependent reduced density matrix. The forward mapping variables are evolved based on the Hamilton's equations of motion[5,33]

$$\dot{q}_i = \partial H_m/\partial p_i;\ \dot{p}_i = -\partial H_m/\partial q_i \tag{4}$$

where $H_m(\mathbf{p}, \mathbf{q}, R) = \frac{P^2}{2M} + \frac{1}{2}\sum_{ij} V_{ij}(R)[p_ip_j + q_iq_j]$ is the PLDM mapping Hamiltonian.[5,33] The backward mapping variables are propagated with the similar equations of motion governed by $H_m(\mathbf{p}', \mathbf{q}', R)$. The nuclei are evolved with the force

$$F = -\frac{1}{4}\sum_{ij}\nabla V_{ij}(R)[p_ip_j + q_iq_j + p'_ip'_j + q'_iq'_j] \tag{5}$$

For a trajectory-based quantum dynamics approach, such as PLDM (as well as SQC[51]), the above equation of motion often requires the energy and nuclear gradients. These quantities can be conveniently evaluated as follows: Consider a short-time propagation of the nuclear DOFs during $t \in [t_0, t_1]$, where the nuclear positions evolve from $R(t_0)$ to $R(t_1)$, and the corresponding adiabatic states are $\{|\Phi_\alpha(R(t_0))\rangle\}$ and $\{|\Phi_\lambda(R(t_1))\rangle\}$. The QD scheme uses the nuclear geometry at time t_0 as a reference geometry, $R_0 \equiv R(t_0)$, and uses the adiabatic basis $\{|\Phi_\alpha(R(t_0))\rangle\}$ as the *quasi-diabatic* basis during this short-time propagation, such that

$$|\Phi_\alpha(R_0)\rangle \equiv |\Phi_\alpha(R(t_0))\rangle,\ \text{for } t \in [t_0, t_1] \tag{6}$$

With the above QD basis defined independent of $R(t)$ within each propagation segment, the derivative couplings vanish while $\hat{V}(R)$ in the QD basis becomes off-diagonal. With this local diabatic basis, all of the necessary diabatic quantities can be evaluated and used to propagate quantum dynamics during $t \in [t_0, t_1]$.

The electronic Hamiltonian operator $\hat{V}(R(t))$ in the QD basis is evaluated as

$$V_{\alpha\beta}(R(t)) = \langle\Phi_\alpha(R_0)|\hat{V}(R(t))|\Phi_\beta(R_0)\rangle \tag{7}$$

DOI: 10.1021/acs.jpclett.9b02747
J. Phys. Chem. Lett. 2019, 10, 7062−7070

For on-the-fly simulations, this quantity is obtained from a linear interpolation[9] between $V_{\alpha\beta}(R(t_0))$ and $V_{\alpha\beta}(R(t_1))$ as

$$V_{\alpha\beta}(R(t)) = V_{\alpha\beta}(R_0) + \frac{(t-t_0)}{(t_1-t_0)}[V_{\alpha\beta}(R(t_1)) - V_{\alpha\beta}(R_0)] \tag{8}$$

where $V_{\alpha\beta}(R_0) = \langle\Phi_\alpha(R_0)|\hat{V}(R(t_0))|\Phi_\beta(R_0)\rangle = E_\alpha(R(t_0))\delta_{\alpha\beta}$. The matrix elements $V_{\alpha\beta}(R(t_1))$ are computed as

$$V_{\alpha\beta}(R(t_1)) = \sum_{\lambda\nu} S_{\alpha\lambda} V_{\lambda\nu}(R(t_1)) S^\dagger_{\beta\nu} \tag{9}$$

where $V_{\lambda\nu}(R(t_1)) = \langle\Phi_\lambda(R(t_1))|\hat{V}(R(t_1))|\Phi_\nu(R(t_1))\rangle = E_\lambda(R(t_1))\delta_{\lambda\nu}$, and the overlap matrix between two adiabatic electronic states (with two different nuclear geometries) are $S_{\alpha\lambda} = \langle\Phi_\alpha(R_0)|\Phi_\lambda(R(t_1))\rangle$ and $S^\dagger_{\beta\nu} = \langle\Phi_\nu(R(t_1))|\Phi_\beta(R_0)\rangle$. These overlap matrices are computed based on the approach outlined in ref 64.

The nuclear gradients $\nabla V_{\alpha\beta}(R(t_1)) \equiv \partial V_{\alpha\beta}(R(t_1))/\partial R$ are evaluated as

$$\begin{aligned}\nabla V_{\alpha\beta}(R(t_1)) &= \nabla\langle\Phi_\alpha(R_0)|\hat{V}(R(t_1))|\Phi_\beta(R_0)\rangle \\ &= \langle\Phi_\alpha(R_0)|\nabla\hat{V}(R(t_1))|\Phi_\beta(R_0)\rangle \\ &= \sum_{\lambda\nu} S_{\alpha\lambda}\langle\Phi_\lambda(R(t_1))|\nabla\hat{V}(R(t_1))|\Phi_\nu(R(t_1))\rangle S^\dagger_{\beta\nu}\end{aligned} \tag{10}$$

Here, we have used the fact that $\{|\Phi_\alpha(R_0)\rangle\}$ is a *diabatic* basis during the $[t_0, t_1]$ propagation, which allows moving the gradient operator to bypass $\langle\Phi_\alpha(R_0)|$. Moreover, we have inserted the resolution of identity $\sum_\lambda|\Phi_\lambda(R(t_1))\rangle\langle\Phi_\lambda(R(t_1))| = 1$ in the second line of eq 10, where we explicitly assume that the QD basis at nuclear position $R(t_1)$ is complete. We emphasize that eq 10 includes derivatives with respect to all possible sources of the nuclear dependence, including those from the adiabatic potentials as well as the adiabatic states.[59,65] The details of this derivation are provided in the Supporting Information.

During the next short-time propagation segment $t \in [t_1, t_2]$, the QD scheme adapts a new reference geometry $R'_0 \equiv R(t_1)$ and new *diabatic* basis $|\Phi_\mu(R'_0)\rangle \equiv |\Phi_\mu(R(t_1))\rangle$, instead of using the old basis $|\Phi_\alpha(R_0)\rangle$. With the nuclear geometry closely following the reference geometry at every single propagation step, the QD basis forms a convenient and compact basis. Note that in principle, one needs infinite crude adiabatic states $\{|\Phi_\alpha(R_0)\rangle\}$ to represent the time-dependent electronic wave function, because the electronic wave function could change rapidly with the motion of the nuclei, and the crude adiabatic basis is convenient only when the nuclear geometry R is close to the reference geometry R_0. By dynamically updating the basis in the QD scheme, the time-dependent electronic wave function is expanded with the "moving crude adiabatic basis"[20] that explores the most relevant and important parts of the Hilbert space, thus explicitly addressing this problem.

On the other hand, the commonly used diabatization schemes (which construct *global* diabatic states) often require a much larger set of the diabatic basis to represent an accurate adiabatic state.[66] We have encountered the same behavior in a photoinduced proton-coupled electron-transfer model system,[65] where 100 strict diabatic states are needed to accurately represent the lowest 10 adiabatic states.[65] However, we emphasize that the quasi-diabatic states (i.e., the moving crude adiabatic states) used here are local diabatic states, not global diabatic states. Thus, we are free of the commonly encountered basis completeness problem in diabatization schemes,[49,66] because we are not trying (nor attempting) to construct global diabatic states. We further emphasize that there is always a nonremovable part of the derivative coupling for polyatomic systems.[2,44,47] Here, the QD scheme circumvents this challenge by requiring only locally defined diabatic states such that the derivative couplings vanish in this configurational subspace around the reference geometry.

Between $[t_0, t_1]$ and $[t_1, t_2]$ propagation segments, all of these quantities will be transformed from $\{|\Phi_\alpha(R_0)\rangle\}$ to $\{|\Phi_\mu(R'_0)\rangle\}$ basis using the relation

$$|\Phi_\lambda(R(t_1))\rangle = \sum_\alpha \langle\Phi_\alpha(R(t_0))|\Phi_\lambda(R(t_1))\rangle|\Phi_\alpha(R(t_0))\rangle \tag{11}$$

When performing the above transformation in eq 11, the eigenvectors maintain their mutual orthogonality subject to a very small error when they are expressed in terms of the previous basis because of the incompleteness of the basis.[56,57] This small numerical error (with a typical value of 10^{-3}–10^{-2} deviating from the strict orthogonality in the current calculation) generated from each step can, however, accumulate over many steps and cause a significant error at longer times, leading to a nonunitary dynamics.[56,57] This problem can be easily resolved by using the Löwdin orthogonalization procedure[67] as commonly used in the local diabatization approach,[56] and this is discussed in detail in the Supporting Information.

Note that the QD propagation scheme does not explicitly require the derivative couplings $d_{\lambda\nu}(R) = \langle\Phi_\lambda(R)|\nabla\Phi_\nu(R)\rangle$ or nonadiabatic couplings $\langle\Phi_\beta(R(t))|\frac{\partial}{\partial t}\Phi_\alpha(R(t))\rangle = d_{\beta\alpha}(R)\dot{R}$. However, the remnants of these quantities do show up in the QD scheme: the nuclear gradient $\nabla V_{\alpha\beta}(R(t_1))$ now contains $\langle\Phi_\lambda(R(t_1))|\nabla\hat{V}(R(t_1))|\Phi_\nu(R(t_1))\rangle$ (see eq 10), which is reminiscent of the derivative coupling because of $\langle\Phi_\lambda|\nabla\hat{V}|\Phi_\nu\rangle = d_{\lambda\nu}(E_\nu - E_\lambda)$, and the QD scheme uses transformation matrix elements $\langle\Phi_\beta(R(t_1))|\Phi_\alpha(R(t_2))\rangle$ instead of $\langle\Phi_\beta(R(t))|\frac{\partial}{\partial t}\Phi_\alpha(R(t))\rangle$. It is worth noting that both $d_{\lambda\nu}(R)$ and $\langle\Phi_\beta(R(t))|\frac{\partial}{\partial t}\Phi_\alpha(R(t))\rangle$ can become singular. The QD scheme explicitly alleviates this difficulty by using well-behaved quantities $\nabla V_{\alpha\beta}(R(t_1))$ and $\langle\Phi_\beta(R(t_1))|\Phi_\alpha(R(t_2))\rangle$. Thus, a method that directly requires derivative couplings and/or nonadiabatic couplings might suffer from numerical instabilities near trivial crossings or conical intersections, with exceptions such as the recently developed norm-preserving interpolation scheme[68,69] that provides a stable integration of TDSE in the adiabatic representation despite the explicit presence of $\langle\Phi_\beta|\frac{\partial}{\partial t}|\Phi_\alpha\rangle$. The QD scheme, on the other hand, uses only well-behaved quantities for propagating quantum dynamics, which thus allows using a much larger nuclear time-step[51] and can significantly reduce the number of required electronic structure calculations that are typically performed at every nuclear time step.

All simulations are performed using a modified version of the SHARC nonadiabatic dynamics interface package,[70,71] with the on-the-fly electronic structure calculations performed with MOLPRO.[72] Computational details of the QD-PLDM and QD-SQC quantum dynamics simulations, a detailed numerical algorithm of the QD propagation scheme, and other technical

DOI: 10.1021/acs.jpclett.9b02747
J. Phys. Chem. Lett. 2019, 10, 7062−7070

details, including system initialization, Wigner initial sampling of the nuclei, the algorithm to track the phase of adiabatic states, and Löwdin orthogonalization, are provided in the Supporting Information.

Results and Discussion. Ethylene exhibits a complex photodissociation dynamics by visiting several conical intersections and undergoing various reaction pathways during the nonradiative decay processes. It is thus considered as a prototype for investigating photoisomerization reactions through conical intersections[3] and has been extensively studied through theoretical[73−78] and experimental[79−82] investigations. To provide an accurate description of the electronic structure of ethylene, we follow the previous theoretical studies[76,83] and use the CASSCF approach that has been shown to provide accurate potential around conical intersections. To avoid the root-flipping problem,[76,77,83] the CASSCF calculations are performed using state-averaging over three states, at the level of SA-3-CASSCF(2,2) with 6-31G* basis set as implemented in MOLPRO.[72] The nonadiabatic dynamics simulation is propagated in the $\{|S_0(R)\rangle,|S_1(R)\rangle\}$ electronic states subspace, i.e., the ground and the first excited states, by using the information from the on-the-fly CASSCF calculations. All of the QD-PLDM and QD-SQC approaches are implemented in a modified version of NAMD interface code SHARC,[70,71] which is used to perform all of the simulations in this Letter.

Figure 1 presents the adiabatic potential energy surface (PES) of ethylene, with both the S_1 state (upper surface) and

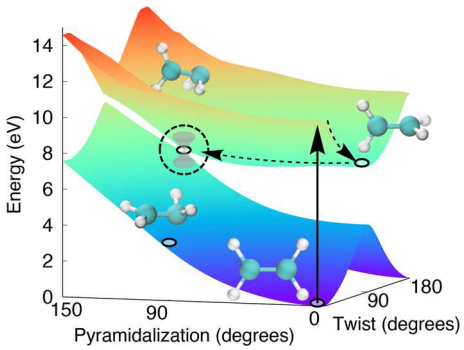

Figure 1. CASSCF potential energy surface of S_1 (upper surface) and S_0 (lower surface) along two main reaction coordinates of photodissociation pathways in ethylene. Upon photoexcitation, the system quickly relaxes to the minimum along the twist angle on the S_1 surface; it then pyramidalizes and relaxes back to the S_0 through the twisted-pyramidalized conical intersection.

S_0 state (lower surface) along the pyramidalization and the twist reaction coordinates, obtained from the PES scanning. The conical intersections between these two surfaces are also indicated with a dotted circle, located at a twist angle of 90° and the pyramidalization angle around 108°. Upon the photoexcitation (indicated by the solid arrow), ethylene first relaxes on the S_1 surface along the twist angle (indicated by the dashed arrow), then pyramidalizes on the S_1 surface and reaches to the region of the conical intersection (which is commonly termed the twisted-pyramidalized conical intersection), and quickly relaxes back to the S_0 surface. This, of course, is only a very simplified picture. The actual nonadiabatic dynamics are much more complex, and a direct on-the-fly NAMD simulation is often necessary to reveal the fundamental mechanistic insights into these complex reaction channels.[3,75,77,81,84]

Figure 2 presents the adiabatic population dynamics obtained from the QD scheme. The CAS adiabatic states (many-electron wave functions) at a reference geometry are used as the diabatic states during a propagation segment, which are then dynamically updated for the subsequent propagation step. In Figure 2A, the canonical orbitals (HOMO and LUMO) of the on-the-fly CAS(2,2) calculations are visualized along a given trajectory that forms the ethylidene structure. This is one of the most likely reactive trajectories at the end of our QD-PLDM simulations (when t = 200 fs), which accounts for more than 40% of all possible reaction pathways. The dynamics are propagated with the PLDM or the SQC approaches, with the results presented in panels B and C of Figure 2, respectively. For comparison, FSSH with decoherence correction[85] and the local-diabatization propagation scheme[56] is also used to generate the photodynamics. For the trajectory-based approaches, a total of 120 trajectories are used to compute the population, with a nuclear time step dt = 0.1 fs, although a much larger time step dt = 0.5 fs can be used to generate nearly identical results at a single-trajectory level. The amount of trajectories used here is sufficient to provide the basic trend of the population dynamics, and the convergence tests with up to 500 trajectories are provided in the Supporting Information. The nuclear initial configurations are sampled from the Wigner distribution of the ground vibrational state (ν = 0) on the ground electronic state S_0, with the harmonic approximation based on the approach outlined in ref 86. The mapping variables (i.e., the electronic DOF) in PLDM and SQC calculations are propagated based on the QD scheme with 200 time steps during each nuclear time step. Additional numerical details of these calculations, the convergence test with an increasing number of trajectories, as well as the energy conservation analysis are provided in the Supporting Information. Further, results obtained from AIMS simulation[77] are presented for comparison. Because AIMS is a wavepacket-based approach which has been extensively tested,[7,16,87] we consider it as an accurate solution for the quantum dynamics of the "CAS ethylene model system" and use it as the benchmark of our calculations. Other recently developed wavepacket approaches, such as the multiconfigurational Ehrenfest (MCE) method, provide essentially the same results as AIMS for this test case at the same level of electronic structure theory.[17]

Figure 2B presents the comparison of the population dynamics obtained from QD-PLDM (solid lines) and the decoherence-corrected FSSH (dashed lines), in addition to AIMS (filled circles) where the data points are directly taken from ref 77. The population differences between the trajectory-based approaches and AIMS are presented in the bottom panel. All three approaches provide the same plateau of the S_1 population (t = 0−20 fs), which corresponds to the initial *adiabatic* nuclear relaxation process on the S_1 surface. During t = 20−75 fs, the system starts to exhibit quick nonadiabatic transitions between S_1 and S_0 states through conical intersections. Here, QD-PLDM agrees reasonably well with AIMS throughout the entire nonradiative decay process. FSSH, on the other hand, predicts a much faster relaxation dynamics and exhibits a large deviation compared to the AIMS, likely caused by the overcoherence problem despite being corrected by a simple decoherence scheme in this calculation. More sophisticated decoherence corrections[12] might further improve the results of FSSH. It is worth noting that the experimentally[81] measured S_1 decay time is ∼89 fs, agreeing

DOI: 10.1021/acs.jpclett.9b02747
J. Phys. Chem. Lett. 2019, 10, 7062−7070

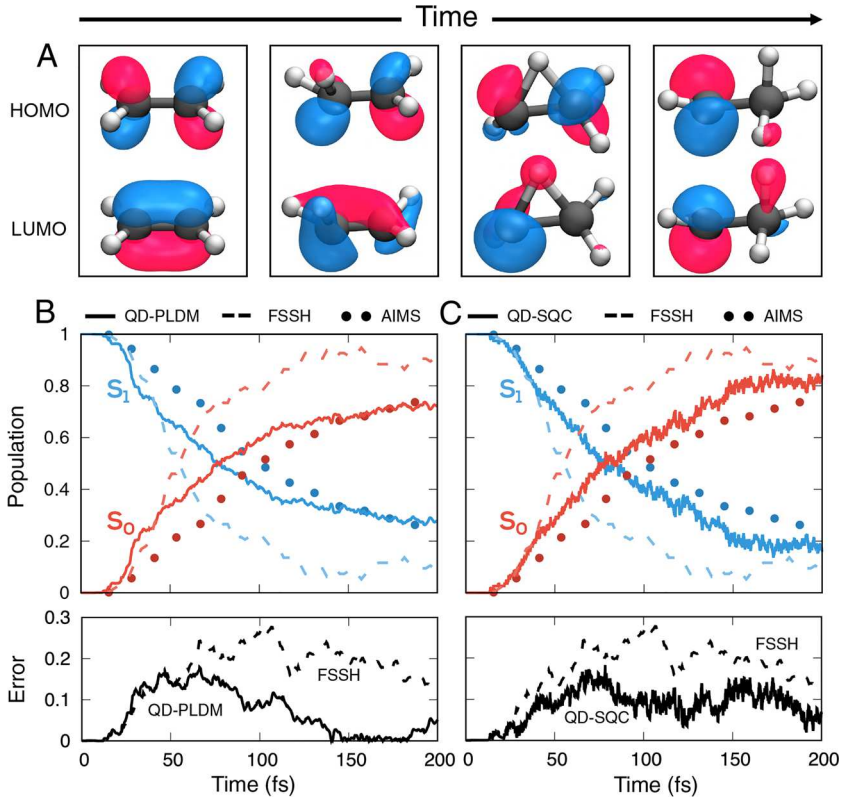

Figure 2. Population dynamics obtained from the QD propagation scheme. (A) Frontier molecular orbitals (HOMO and LUMO canonical orbitals) along a given nuclear trajectory. (B) Adiabatic electronic populations of S_1 (blue) and S_0 (red) obtained from QD-PLDM (solid lines), FSSH (dashed lines), and AIMS (filled circles) with data points taken from ref 77, respectively. AIMS, which is an approximate Gaussian wavepacket-based nonadiabatic method, is used as the benchmark result. The bottom panel presents the time-dependent error between the trajectory-based approach and AIMS. (C) Adiabatic electronic populations obtained from QD-SQC (solid lines), with the rest same as presented in panel B.

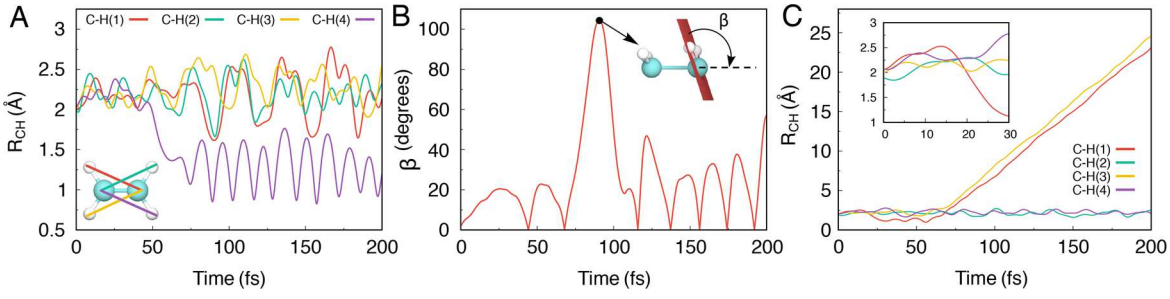

Figure 3. Representative QD-PLDM reactive trajectories for (A) hydrogen transfer, (B) pyramidalization, and (C) H_2 dissociation pathways. The C−H bond lengths are defined in the inset of panel A and are used in both panels A and C. The pyramidalization angle is defined in the inset of panel B.

well with the AIMS value when using the CASPT2 level of the electronic structure calculations that include dynamical correlation.[77] Our intention in this Letter, on the other hand, is not trying to compare to or recover the experimental results, but rather comparison to the "CAS(2,2) ethylene model" provided by AIMS. We emphasize that the AIMS results should be viewed only as an approximate (yet accurate) solution of the TDSE of the system. Numerically exact simulations (based on the MCTDH calculations) for ethylene diabatic models[66,88] have been performed. The numerically exact solution for this CAS(2,2) model as the ultimate theoretical benchmark is likely to be obtained with on-the-fly simulations through the direct-dynamics MCTDH approach.[30,49]

Figure 2C presents a similar comparison of the population dynamics obtained from QD-SQC (solid lines), the decoherence corrected FSSH (dashed lines), and AIMS (filled circles) with the difference between the trajectory-based approaches and AIMS provided in the bottom panel. Here, we choose to use the simplest possible square window function[60] proposed by Cotton and Miller. The QD-SQC provides a similar level of accuracy for the population dynamics compared to QD-PLDM and agrees reasonably well with AIMS throughout the nonradiative decay process. A slightly noisy population is obtained because only a fraction of the mapping trajectories landed in all population windows at any given time, thus reducing the quality of the data and at the same time requiring normalization of the population.[60] The detailed analysis of the

DOI: 10.1021/acs.jpclett.9b02747
J. Phys. Chem. Lett. 2019, 10, 7062−7070

fraction of mapping trajectories landing outside both windows is provided in the Supporting Information. Nevertheless, QD-SQC still outperforms FSSH in this on-the-fly CAS(2,2) model. We note that more accurate results for model systems can be obtained by using triangle windows[89] and the trajectory-specific zero-point energy correction technique.[90] These new developments will be investigated through the ab initio NAMD simulations by using the QD scheme. Through results presented here, we demonstrate that the QD scheme enables many possibilities of using recently developed diabatic quantum dynamics approaches for accurate ab initio on-the-fly NAMD simulations with the adiabatic electronic structure calculations. Further, the QD propagation scheme also provides new opportunities to assess the performance of approximate diabatic dynamics approaches, with ab initio test cases beyond simple diabatic model systems.

Figure 3 presents three representative reactive trajectories obtained from QD-PLDM, whereas the averaged populations of different nuclear configurations are provided in Figure 4. A

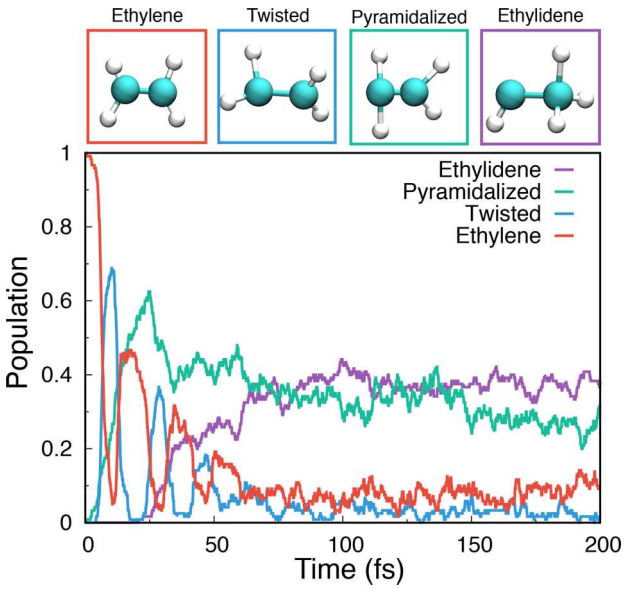

Figure 4. Population dynamics of various dissociation products obtained from the QD-PLDM simulations, with representative geometries presented in the top panels.

qualitatively similar ensemble of reactive trajectories are also obtained from QD-SQC (not shown). These reactive trajectories provide intuitive time-dependent mechanistic insights into the competing nonradiative decay channels, although a physically meaningful interpretation should be drawn only from the expectation values (such as those presented in Figure 4). Figure 3A presents the time-evolution of the bond distance between carbon and hydrogen atoms that are not initially bonded. At $t \approx 50$ fs, one of these four distances suddenly drops from ~2.2 to ~1.25 Å, indicating the formation of an ethylidene structure through the ethylidene-like conical intersection[77] (which is different than the twisted-pyramidalized conical intersection shown in Figure 1). Figure 3B presents the time evolution of the (modulus of) pyramidalization angle defined in the inset of this panel, forming a persisting oscillation pattern. The zero value of the angle indicates that the molecule goes through the planar structure and vibrates on the other side of the molecular plane. The inset provides the structure of the largest pyramidalization angle at ≈100°, which is close to the twisted-pyramidalized conical intersection[74] shown in Figure 1. Figure 3C presents a reactive trajectory of H_2 dissociation, which occurs at $t \approx 70$ fs after one H atom abstraction process, as can be seen from the inset of this panel (C−H(1) bond length shrinking indicated by the red curve). These reactive trajectories are in a close agreement with the similar reactive channels discovered from the AIMS simulation.[76,77]

Figure 4 presents the population of various nuclear configurations obtained from QD-PLDM through the ensemble average of trajectories. These nuclear configurations are defined based on the criteria in ref 84, with the representative geometries provided in the top of this figure (squared with the same color coding used in the population curve). At the short time $t \in [0, 20]$ fs, the system evolves adiabatically on the S_1 surface, moving along both the twisted and pyramidalized reaction coordinates, accumulating the population for both configurations. The twisted configuration on S_1 also converts into the pyramidalized configuration during this time. Note that the oscillation period of twisted configuration is around 20 fs, consistent with results obtained from AIMS[76] and MCE approaches.[17] After the early time relaxation on the S_1 surface, the system exhibits various conical intersections and makes a nonadiabatic transition to the S_0 surface, relaxing back to the ethylene configuration (red), ending up with ethylidene configuration (magenta), or dissociating H_2 out of ethylene (with only 8 reactive trajectories out of 120 trajectories, and thus not shown in this figure). Our QD-PLDM simulation predicts that about 50% of the molecules go through the ethylidene-like conical intersection and that the other 50% of the molecules go through the twisted-pyramidalized conical intersection, which agrees well with the AIMS results performed at the CASSCF level of theory.[76,77]

Conclusions. In this Letter, we provide the first ab initio on-the-fly example of using the QD scheme[50] for nonadiabatic simulations with *diabatic* quantum dynamics approaches. With two recently developed diabatic dynamics approaches (PLDM and SQC) and on-the-fly CASSCF calculations, we simulate the on-the-fly nonadiabatic dynamics of the ethylene photodeactivation process. During each short-time propagation segment, the adiabatic states associated with a reference geometry are used as the quasi-diabatic (local diabatic) states, allowing any diabatic dynamics approach to propagate the quantum dynamics during this time step. Between two consecutive propagation segments, the definition of the quasi-diabatic states is updated. The QD scheme thus allows a direct interface between diabatic trajectory-based quantum dynamics approaches with adiabatic electronic structure calculations and completely eliminates the necessity of any representation reformulating efforts, such as constructing global diabatic states through diabatization or reformulating the diabatic dynamics approach to adiabatic representation.

The results obtained from both QD-PLDM and QD-SQC are in close agreement with AIMS; both outperform the widely used FSSH approach. The QD scheme thus enables many recently developed diabatic quantum dynamics approaches for ab inito on-the-fly simulations, providing the nonadiabatic community a wide variety of approaches (such as PLDM and SQC) beyond the well-explored methods (such as trajectory surface-hopping or ab initio multiple-spawning methods). Further, the QD scheme also enables using realistic test cases

DOI: 10.1021/acs.jpclett.9b02747
J. Phys. Chem. Lett. 2019, 10, 7062−7070

that go beyond simple model systems to assess the accuracy and limitations of recently developed quantum dynamics approaches and will foster the development of new quantum dynamics approaches.

This work completes the establishment of the QD scheme in the field of ab initio nonadiabatic dynamics simulation, demonstrating the QD scheme as a powerful tool to enable accurate diabatic quantum dynamics approaches for on-the-fly simulations. The development of the QD scheme provides a valuable addition to the existing quantum dynamics approaches that rely on building the on-the-fly diabatic representation, such as the direct-dynamics variational multiconfiguration Gaussian method[49] or direct-dynamics MCTDH approach.[26−30] It also sends out the following assuring messages to the quantum dynamics community: (i) To propagate quantum dynamics with diabatic dynamics approaches, one needs only *locally* well-defined diabatic states (in this case, the moving crude adiabatic basis[20]), as opposed to the *global* diabatic states obtained from diabatization procedures.[2,43−49] (ii) A diabatic dynamics approach can be directly interfaced with adiabatic electronic structure calculations to perform on-the-fly simulations without additional representation reformulating efforts.[91−93]

■ ASSOCIATED CONTENT

Supporting Information

The Supporting Information is available free of charge on the ACS Publications website at DOI: 10.1021/acs.jpclett.9b02747.

A brief introduction of the SQC approach; details of the QD propagation algorithm; details of the QD nuclear gradient derivation; numerical details of the on-the-fly calculations for QD-PLDM, QD-SQC, and FSSH; additional results for convergence with increasing number of trajectories, energy conservation analysis, and the mapping trajectories anaylsis in QD-SQC calculations (PDF)

■ AUTHOR INFORMATION

Corresponding Author

*E-mail: pengfei.huo@rochester.edu.

ORCID

Pengfei Huo: 0000-0002-8639-9299

Notes

The authors declare no competing financial interest.

■ ACKNOWLEDGMENTS

This work was supported by the National Science Foundation CAREER Award under Grant No. CHE-1845747 as well as by "Enabling Quantum Leap in Chemistry" program under Grant CHE-1836546. W.Z. appreciates the support from the China Scholarship Council (CSC) during his visit at the University of Rochester. A.M. appreciates the support from his Elon Huntington Hooker Fellowship. Computing resources were provided by the Center for Integrated Research Computing (CIRC) at the University of Rochester. W.Z. appreciates valuable discussions with Daniel Hollas. We appreciate the generous technical support and valuable and timely feedback from the SHARC developer team by Dr. Sebastian Mai and Prof. Leticia Gonzàlez. P.H. appreciates valuable discussions with Profs. Ben Levine, Artur Izmaylov, and Dmitry Shalashilin, as well as the encouragement from Prof. Bill Miller that initiated this work.

■ REFERENCES

(1) Tully, J. C. Perspective: Nonadiabatic dynamics theory. *J. Chem. Phys.* **2012**, *137*, 22A301.

(2) Subotnik, J. E.; Alguire, E. C.; Ou, Q.; Landry, B. R.; Fatehi, S. The Requisite Electronic Structure Theory to Describe Photoexcited Nonadiabatic Dynamics: Nonadiabatic Derivative Couplings and Diabatic Electronic Couplings. *Acc. Chem. Res.* **2015**, *48*, 1340−1350.

(3) Levine, B. G.; Martinez, T. J. Isomerization Through Conical Intersections. *Annu. Rev. Phys. Chem.* **2007**, *58*, 613−634.

(4) Nelson, T.; Fernandez-Alberti, S.; Roitberg, A. E.; Tretiak, S. Nonadiabatic Excited-State Molecular Dynamics: Modeling Photophysics in Organic Conjugated Materials. *Acc. Chem. Res.* **2014**, *47*, 1155−1164.

(5) Lee, M. K.; Huo, P.; Coker, D. F. Semiclassical Path Integral Dynamics: Photosynthetic Energy Transfer with Realistic Environment Interactions. *Annu. Rev. Phys. Chem.* **2016**, *67*, 639−668.

(6) Crespo-Otero, R.; Barbatti, M. Recent Advances and Perspectives on Nonadiabatic Mixed Quantum-Classical Dynamics. *Chem. Rev.* **2018**, *118*, 7026−7068.

(7) Curchod, B. F. E.; Martinez, T. J. Ab initio Nonadiabatic Quantum Molecular Dynamics. *Chem. Rev.* **2018**, *118*, 3305−3336.

(8) Tully, J. C. Molecular dynamics with Electronic Transitions. *J. Chem. Phys.* **1990**, *93*, 1061−1071.

(9) Webster, F.; Rossky, P. J.; Friesner, R. A. Nonadiabatic Processes in Condensed Matter: Semi-Classical Theory and Implementation. *Comput. Phys. Commun.* **1991**, *63*, 494−522.

(10) Space, B.; Coker, D. Nonadiabatic Dynamics of Excited Excess Electrons in Simple Fluids. *J. Chem. Phys.* **1991**, *94*, 1976−1984.

(11) Hammes-Schiffer, S.; Tully, J. C. Proton Transfer in Solution: Molecular Dynamics with Quantum Transitions. *J. Chem. Phys.* **1994**, *101*, 4657−4667.

(12) Subotnik, J. E.; Jain, A.; Landry, B.; Petit, A.; Ouyang, W.; Bellonzi, N. Understanding the Surface Hopping View of Electronic Transitions and Decoherence. *Annu. Rev. Phys. Chem.* **2016**, *67*, 387−417.

(13) Tapavicza, E.; Tavernelli, I.; Rothlisberger, U. Trajectory Surface Hopping within Linear Response Time-Dependent Density-Functional Theory. *Phys. Rev. Lett.* **2005**, *98*, DOI: 10.1103/PhysRevLett.98.023001.

(14) Wang, L.; Akimov, A.; Prezhdo, O. V. Recent Progress in Surface Hopping: 2011−2015. *J. Phys. Chem. Lett.* **2016**, *7*, 2100−2112.

(15) Barbatti, M. Nonadiabatic Dynamics with Trajectory Surface Hopping Method. *Wiley Int. Rev. Comp. Mol. Sci.* **2011**, *1*, 620−633.

(16) Ben-Nun, M.; Quenneville, J.; Martinez, T. J. Ab Initio Multiple Spawning: Photochemistry from First Principles Quantum Molecular Dynamics. *J. Phys. Chem. A* **2000**, *104*, 5161−5175.

(17) Saita, K.; Shalashilin, D. V. On-the-fly ab initio molecular dynamics with multiconfigurational Ehrenfest method. *J. Chem. Phys.* **2012**, *137*, 22A506.

(18) Makhov, D. V.; Glover, W. J.; Martinez, T. J.; Shalashilin, D. V. Ab Initio Multiple Cloning Algorithm for Quantum Nonadiabatic Molecular Dynamics. *J. Chem. Phys.* **2014**, *141*, 054110.

(19) Fernandez-Alberti, S.; Makhov, D. V.; Tretiak, S.; Shalashilin, D. V. Non-Adiabatic Excited State Molecular Dynamics of Phenylene Ethynylene Dendrimer Using a Multiconfigurational Ehrenfest Approach. *Phys. Chem. Chem. Phys.* **2016**, *18*, 10028.

(20) Joubert-Doriol, L.; Izmaylov, A. F. Variational Nonadiabatic Dynamics in the Moving Crude Adiabatic Representation: Further Merging of Nuclear Dynamics and Electronic Structure. *J. Chem. Phys.* **2018**, *148*, 114102.

(21) Meek, G. A.; Levine, B. G. The Best of Both Reps-Diabatized Gaussians on Adiabatic Surfaces. *J. Chem. Phys.* **2016**, *145*, 184103.

(22) Min, S. K.; Agostini, F.; Tavernelli, O.; Gross, E. K. U. Ab Initio Nonadiabatic Dynamics with Coupled Trajectories: A Rigorous

DOI: 10.1021/acs.jpclett.9b02747
J. Phys. Chem. Lett. 2019, 10, 7062−7070

Approach to Quantum (De)Coherence. *J. Phys. Chem. Lett.* **2017**, *8*, 3048−3055.
(23) Curchod, B. F.; Agostini, F.; Tavernelli, I. CT-MQC−a coupled-trajectory mixed quantum/classical method including non-adiabatic quantum coherence effects. *Eur. Phys. J. B* **2018**, *91*, 168.
(24) Sato, S. A.; Kelly, A.; Rubio, A. Coupled forward-backward trajectory approach for nonequilibrium electron-ion dynamics. *Phys. Rev. B: Condens. Matter Mater. Phys.* **2018**, *97*, 134308.
(25) Martens, C. C. Surface Hopping by Consensus. *J. Phys. Chem. Lett.* **2016**, *7*, 2610−2615.
(26) Worth, G. A.; Robb, M. A.; Burghardt, I. A novel algorithm for non-adiabatic direct dynamics using variational Gaussian wavepackets. *Faraday Discuss.* **2004**, *127*, 307−323.
(27) Allan, C. S. M.; Lasorne, B.; Worth, G. A.; Robb, M. A. A Straightforward Method of Analysis for Direct Quantum Dynamics: Application to the Photochemistry of a Model Cyanine. *J. Phys. Chem. A* **2010**, *114*, 8713−8729.
(28) Richings, G. W.; Worth, G. A. Multi-state non-adiabatic direct-dynamics on propagated diabaticpotential energy surfaces. *Chem. Phys. Lett.* **2017**, *683*, 606−612.
(29) Richings, G. W.; Habershon, S. MCTDH on-the-fly: Efficient grid-based quantum dynamics without pre-computed potential energy surfaces. *J. Chem. Phys.* **2018**, *148*, 134116.
(30) Richings, G. W.; Robertson, C.; Habershon, S. Improved on-the-fly MCTDH simulations with many-body-potential tensor decomposition and projection diabatisation. *J. Chem. Theory Comput.* **2019**, *15*, 857−870.
(31) Schmidt, J. R.; Parandekar, P. V.; Tully, J. C. Mixed Quantum-Classical Euilibrium: Surface Hopping. *J. Chem. Phys.* **2008**, *129*, 044104.
(32) Kelly, A.; van Zon, R.; Schofield, J.; Kapral, R. Mapping Quantum-Classical Liouville Equation: Projectors and Trajectories. *J. Chem. Phys.* **2012**, *136*, 084101.
(33) Huo, P.; Coker, D. F. Communication: Partial Linearized Density Matrix Dynamics for Dissipative, Non-Adiabatic Quantum Evolution. *J. Chem. Phys.* **2011**, *135*, 201101.
(34) Hsieh, C.-Y.; Kapral, R. Analysis of the Forward-Backward Trajectory Solution for the Mixed Quantum-Classical Liouville Equation. *J. Chem. Phys.* **2013**, *138*, 134110.
(35) Walters, P. L.; Makri, N. Iterative Quantum-Classical Path Integral with Dynamically Consistent State Hopping. *J. Chem. Phys.* **2016**, *144*, 044108.
(36) Ananth, N. Mapping Variable Ring Polymer Molecular Dynamics: A Path-Integral Based Method for Nonadiabatic Processes. *J. Chem. Phys.* **2013**, *139*, 124102.
(37) Richardson, J. O.; Thoss, M. Communication: Nonadiabatic Ring-Polymer Molecular Dynamics. *J. Chem. Phys.* **2013**, *139*, 031102.
(38) Chowdhury, S. N.; Huo, P. Coherent State Mapping Ring-Polymer Molecular Dynamics for Non-Adiabatic Quantum Propagations. *J. Chem. Phys.* **2017**, *147*, 214109.
(39) Miller, W. H.; Cotton, S. J. Classical Molecular Dynamics Simulation of Electronically Non-Adiabatic Processes. *Faraday Discuss.* **2016**, *195*, 9−30.
(40) Miller, W. H.; Cotton, S. J. Communication: Note on detailed balance in symmetrical quasi-classical models for electronically non-adiabatic dynamics. *J. Chem. Phys.* **2015**, *142*, 131103.
(41) Mulvihill, E.; Schubert, A.; Sun, X.; Dunietz, B. D.; Geva, E. A modified approach for simulating electronically nonadiabatic dynamics via the generalized quantum master equation. *J. Chem. Phys.* **2019**, *150*, 034101.
(42) Saller, M. A. C.; Kelly, A.; Richardson, J. O. On the identity of the identity operator in nonadiabatic linearized semiclassical dynamics. *J. Chem. Phys.* **2019**, *150*, 071101.
(43) Baer, M. Adiabatic and Diabatic Representations for Atom-Diatom Collisions: Treatment of the Three-Dimensional Case. *Chem. Phys.* **1976**, *15*, 49−57.
(44) Mead, C. A.; Truhlar, D. G. Conditions for the Definition of a Strictly Diabatic Electronic Basis for Molecular Systems. *J. Chem. Phys.* **1982**, *77*, 6090.
(45) Cave, R. J.; Newton, M. D. Calculation of electronic coupling matrix elements for ground and excited state electron transfer reactions: Comparison of the generalized Mulliken-Hush and block diagonalization methods. *J. Chem. Phys.* **1997**, *106*, 9213.
(46) Subotnik, J. E.; Yeganeh, S.; Cave, R. J.; Ratner, M. A. Constructing Diabatic States from Adiabatic States: Extending Generalized Mulliken-Hush to Multiple Charge Centers with Boys Localization. *J. Chem. Phys.* **2008**, *129*, 244101.
(47) Van Voorhis, T.; Kowalczyk, T.; Kaduk, B.; Wang, L.-P.; Cheng, C.-L.; Wu, Q. The Diabatic Picture of Electron Transfer, Reaction Barriers, and Molecular Dynamics. *Annu. Rev. Phys. Chem.* **2010**, *61*, 149−170.
(48) Guo, H.; Yarkony, D. R. Accurate Nonadiabatic Dynamics. *Phys. Chem. Chem. Phys.* **2016**, *18*, 26335−26352.
(49) Richings, G. W.; Worth, G. A. A Practical Diabatisation Scheme for Use with the Direct-Dynamics Variational Multi-Configuration Gaussian Method. *J. Phys. Chem. A* **2015**, *119*, 12457−12470.
(50) Mandal, A.; Yamijala, S.; Huo, P. Quasi Diabatic Representation for Nonadiabatic Dynamics Propagation. *J. Chem. Theory Comput.* **2018**, *14*, 1828−1840.
(51) Sandoval C, J. S.; Mandal, A.; Huo, P. Symmetric Quasi Classical Dynamics with Quasi Diabatic Propagation Scheme. *J. Chem. Phys.* **2018**, *149*, 044115.
(52) Choi, H.; Baeck, K. K.; Martinez, T. J. Ab initio equation-of-motion coupled-cluster molecular dynamics with on-the-fly diabatization: the doublet-like feature in the photoabsorption spectrum of ethylene. *Chem. Phys. Lett.* **2004**, *398*, 407−413.
(53) Pacher, T.; Cederbaum, L. S.; Köppel, H. Approximately diabatic states from block diagonalization of the electronic Hamiltonian. *J. Chem. Phys.* **1988**, *89* (1988), 7367−7381.
(54) Yu, N.; Margulis, C.; Coker, D. Influence of Solvation Environment on Excited State Avoided Crossings and Photodissociation Dynamics. *J. Phys. Chem. B* **2001**, *105*, 6728−6737.
(55) Rego, L. G.; Batista, V. S. Quantum Dynamics Simulations of Interfacial Electron Transfer in Sensitized TiO2 Semiconductors. *J. Am. Chem. Soc.* **2003**, *125*, 7989−7997.
(56) Granucci, G.; Persico, M.; Toniolo, A. Direct semiclassical simulation of photochemical processes with semiempirical wave functions. *J. Chem. Phys.* **2001**, *114*, 10608−10615.
(57) Plasser, F.; Granucci, G.; Pittner, J.; Barbatti, M.; Persico, M.; Lischka, H. Surface Hopping Dynamics using a Locally Diabatic Formalism: Charge Transfer in the Ethylene Dimer Cation and Excited State Dynamics in the 2-Pyridone Dimer. *J. Chem. Phys.* **2012**, *137*, 22A514.
(58) Meek, G. A.; Levine, B. G. Wave function continuity and the diagonal Born-Oppenheimer correction at conical intersections. *J. Chem. Phys.* **2016**, *144*, 184109.
(59) Mandal, A.; Sandoval C, J. S.; Shakib, F. A.; Huo, P. Quasi-Diabatic Propagation Scheme for Direct Simulation of Proton−Coupled Electron Transfer Reaction. *J. Phys. Chem. A* **2019**, *123*, 2470−2482.
(60) Cotton, S. J.; Miller, W. H. Symmetrical Windowing for Quantum States in Quasi-Classical Trajectory Simulations: Application to electronically non-adiabatic processes. *J. Chem. Phys.* **2013**, *139*, 234112.
(61) Meyer, H.-D.; Miller, W. H. A Classical Analog for Electronic Degrees of Freedom in Nonadiabatic Collision Processes. *J. Chem. Phys.* **1979**, *70*, 3214−3223.
(62) Stock, G.; Thoss, M. Semiclassical Description of Nonadiabatic Quantum Dynamics. *Phys. Rev. Lett.* **1997**, *78*, 578−581.
(63) Thoss, M.; Stock, G. Mapping Approach to the Semiclassical Description of Nonadiabatic Quantum Dynamics. *Phys. Rev. A: At., Mol., Opt. Phys.* **1999**, *59*, 64−79.
(64) Plasser, F.; Ruckenbauer, M.; Mai, S.; Oppel, M.; Marquetand, P.; Gonzàlez, L. Efficient and Flexible Computation of Many-Electron Wave Function Overlaps. *J. Chem. Theory Comput.* **2016**, *12*, 1207−1219.

DOI: 10.1021/acs.jpclett.9b02747
J. Phys. Chem. Lett. 2019, 10, 7062−7070

(65) Mandal, A.; Shakib, F. A.; Huo, P. Investigating Photoinduced Proton Coupled Electron Transfer Reaction using Quasi Diabatic Dynamics Propagation. *J. Chem. Phys.* **2018**, *148*, 244102.
(66) Jornet-Somoza, J.; Lasorne, B.; Robb, M. A.; Meyer, H.-D.; Lauvergnat, D.; Gatti, F. A generalised 17-state vibronic-coupling Hamiltonian model for ethylene. *J. Chem. Phys.* **2012**, *137*, 084304.
(67) Löwdin, P. O. On the NonOrthogonality Problem Connected with the Use of Atomic Wave Functions in the Theory of Molecules and Crystals. *J. Chem. Phys.* **1950**, *18*, 365−375.
(68) Meek, G. A.; Levine, B. G. Evaluation of the Time-Derivative Coupling for Accurate Electronic State Transition Probabilities from Numerical Simulations. *J. Phys. Chem. Lett.* **2014**, *5*, 2351−2356.
(69) Jain, A.; Alguire, E.; Subotnik, J. E. An Efficient, Augmented Surface Hopping Algorithm That Includes Decoherence for Use in Large-Scale Simulations. *J. Chem. Theory Comput.* **2016**, *12*, 5256−5268.
(70) Mai, S.; Marquetand, P.; Gonzalez, L. Nonadiabatic dynamics: The SHARC approach. *WIREs Comput. Mol. Sci.* **2018**, *8*, 1370.
(71) Mai, S.; Marquetand, P.; Gonzalez, L. General Method to Describe Intersystem Crossing Dynamics in Trajectory Surface Hopping. *Int. J. Quantum Chem.* **2015**, *115*, 1215−1231.
(72) Werner, H.-J.; Knowles, P. J.; Knizia, G.; Manby, F. R.; Schütz, M. Molpro: a general-purpose quantum chemistry program package. *WIREs Comput. Mol. Sci.* **2012**, *2*, 242−253.
(73) Ben-Nun, M.; Martínez, T. J. Ab initio molecular dynamics study of *cis-trans* photoisomerization in ethylene. *Chem. Phys. Lett.* **1998**, *298*, 57−65.
(74) Barbatti, M.; Paier, J.; Lischka, H. Photochemistry of ethylene: A multireference configuration interaction investigation of the excited-state energy surface. *J. Chem. Phys.* **2004**, *121*, 11614.
(75) Barbatti, M.; Granucci, G.; Persico, M.; Lischka, H. Semiempirical molecular dynamics investigation of the excited state lifetime of ethylene. *Chem. Phys. Lett.* **2005**, *401*, 276−281.
(76) Levine, B. G.; Coe, J. D.; Virshup, A. M.; Martínez, T. J. Implementation of ab initio multiple spawning in the MOLPRO quantum chemistry package. *Chem. Phys.* **2008**, *347*, 3−16.
(77) Tao, H.; Levine, B. G.; Martínez, T. J. Ab initio multiple spawning dynamics using multi-state second-order perturbation theory. *J. Phys. Chem. A* **2009**, *113*, 13656−13662.
(78) Mori, T.; Glover, W. J.; Schuurman, M. S.; Martínez, T. J. Role of Rydberg States in the photochemical dynamics of ethylene. *J. Phys. Chem. A* **2012**, *116*, 2808−2818.
(79) Kosma, K.; Trushin, S. A.; Fuss, W.; Schmid, W. E. Ultrafast dynamics and coherent oscillations in ethylene and ethylene-d_4 excited at 162 nm. *J. Phys. Chem. A* **2008**, *112*, 7514−7529.
(80) Kobayashi, T.; Horio, T.; Suzuki, T. Ultrafast deactivation of the $\pi\pi^*(V)$state of ethylene studied using sub-20 fs time-resolved photoelectron imaging. *J. Phys. Chem. A* **2015**, *119*, 9518−9523.
(81) Tao, H.; Allison, T. K.; Wright, T. W.; Stooke, A. M.; Khurmi, C.; van Tilborg, J.; Liu, Y.; Falcone, R. W.; Belkacem, A.; Martínez, T. J. Ultrafast internal conversion in ethylene. i. The excited state lifetime. *J. Chem. Phys.* **2011**, *134*, 244306.
(82) Allison, T. K.; Tao, H.; Glover, W. J.; Wright, T. W.; Stooke, A. M.; Khurmi, C.; van Tilborg, J.; Liu, Y.; Falcone, R. W.; Martínez, T. J.; Belkacem, A. Ultrafast internal conversion in ethylene. ii. Mechanisms and pathways for quenching and hydrogen elimination. *J. Chem. Phys.* **2012**, *136*, 124317.
(83) Hollas, D.; Šištík, L.; Hohenstein, E. G.; Martínez, T. J.; Slavíček, P. Nonadiabatic Ab Initio Molecular Dynamics with the Floating Occupation Molecular Orbital-Complete Active Space Configuration Interaction Method. *J. Chem. Theory Comput.* **2018**, *14*, 339−350.
(84) Barbatti, M.; Ruckenbauer, M.; Lischka, H. The photodynamics of ethylene: A surface-hopping study on structural aspects. *J. Chem. Phys.* **2005**, *122*, 174307.
(85) Granucci, G.; Persico, M. Critical appraisal of the fewest switches algorithm for surface hopping. *J. Chem. Phys.* **2007**, *126*, 134114.
(86) Sun, L.; Hase, W. L. Comparisons of classical and Wigner sampling of transition state energy levels for quasiclassical trajectory chemical dynamics simulations. *J. Chem. Phys.* **2010**, *133*, 044313.
(87) Ben-Nun, M.; Martínez, T. J. Nonadiabatic molecular dynamics: Validation of the multiple spawning method for a multidimensional problem. *J. Chem. Phys.* **1998**, *108*, 7244−7257.
(88) Brill, M. R.; Gatti, F.; Lauvergnat, D.; Meyer, H.-D. Photoinduced nonadiabatic dynamics of ethene: Six-dimensional wave packet propagations using two different approximations of the kinetic energy operator. *Chem. Phys.* **2007**, *338*, 186−199.
(89) Cotton, S. J.; Miller, W. H. A symmetrical quasi-classical windowing model for the molecular dynamics treatment of non-adiabatic processes involving many electronic states. *J. Chem. Phys.* **2019**, *150*, 104101.
(90) Cotton, S.; Miller, W. Trajectory-adjusted electronic zero point energy in classical Meyer-Miller vibronic dynamics: Symmetrical quasiclassical application to photodissociation. *J. Chem. Phys.* **2019**, *150*, 194110.
(91) Cotton, S. J.; Liang, R.; Miller, W. H. On the Adiabatic Representation of Meyer-Miller Electronic-Nuclear Dynamics. *J. Chem. Phys.* **2017**, *147*, 064112.
(92) Hsieh, C.-Y.; Schofield, J.; Kapral, R. Forward-backward solution of the quantum-classical Liouville equation in the adiabatic mapping basis. *Mol. Phys.* **2013**, *111*, 3546−3554.
(93) Huo, P.; Coker, D. F. Consistent Schemes for Non-Adiabatic Dynamics Derived from Partial Linearized Density Matrix Propagation. *J. Chem. Phys.* **2012**, *137*, 22A535.

DOI: 10.1021/acs.jpclett.9b02747
J. Phys. Chem. Lett. 2019, 10, 7062−7070